Cellular/Molecular

Distinct Roles for Two Histamine Receptors (*hclA* and *hclB*) at the *Drosophila* Photoreceptor Synapse

Antonios Pantazis,[1] Ashvina Segaran,[1] Che-Hsiung Liu,[1] Anton Nikolaev,[2] Jens Rister,[3] Andreas S. Thum,[3] Thomas Roeder,[4] Eugene Semenov,[5] Mikko Juusola,[2] and Roger C. Hardie[1]

[1]Department of Physiology, Development, and Neuroscience, University of Cambridge, Cambridge CB2 3DY, United Kingdom, [2]Department of Biomedical Science, University of Sheffield, Sheffield S10 2TN, United Kingdom, [3]Lehrstuhl für Genetik und Neurobiologie, Universität Würzburg, 97074 Würzburg, Germany, [4]Zoologisches Institut, Abteilung Zoophysiologie, Christian-Albrechts-Universität, D-24098 Kiel, Germany, and [5]Department of Molecular Neurobiology, Drosophila Neurogenetics Laboratory, Institute of Molecular Biology, Bulgarian Academy of Sciences, Sofia 1113, Bulgaria

Histamine (HA) is the photoreceptor neurotransmitter in arthropods, directly gating chloride channels on large monopolar cells (LMCs), postsynaptic to photoreceptors in the lamina. Two histamine-gated channel genes that could contribute to this channel in *Drosophila* are *hclA* (also known as *ort*) and *hclB* (also known as *hisCl1*), both encoding novel members of the Cys-loop receptor superfamily. *Drosophila* S2 cells transfected with these genes expressed both homomeric and heteromeric histamine-gated chloride channels. The electrophysiological properties of these channels were compared with those from isolated *Drosophila* LMCs. HCLA homomers had nearly identical HA sensitivity to the native receptors (EC_{50} = 25 μM). Single-channel analysis revealed further close similarity in terms of single-channel kinetics and subconductance states (~25, 40, and 60 pS, the latter strongly voltage dependent). In contrast, HCLB homomers and heteromeric receptors were more sensitive to HA (EC_{50} = 14 and 1.2 μM, respectively), with much smaller single-channel conductances (~4 pS). Null mutations of *hclA* (ort^{US6096}) abolished the synaptic transients in the electroretinograms (ERGs). Surprisingly, the ERG "on" transients in *hclB* mutants transients were approximately twofold enhanced, whereas intracellular recordings from their LMCs revealed altered responses with slower kinetics. However, HCLB expression within the lamina, assessed by both a GFP (green fluorescent protein) reporter gene strategy and mRNA tagging, was exclusively localized to the glia cells, whereas HCLA expression was confirmed in the LMCs. Our results suggest that the native receptor at the LMC synapse is an HCLA homomer, whereas HCLB signaling via the lamina glia plays a previously unrecognized role in shaping the LMC postsynaptic response.

Key words: **ligand-gated ion channel; chloride channel; retina; vision; LMC; lamina; glia; ort**

Introduction

Histamine (HA) is established as a fast neurotransmitter in the visual system (Elias and Evans, 1983; Hardie, 1987; Callaway and Stuart, 1989; Sarthy, 1991), and some mechanosensory circuits (Buchner et al., 1993) of many arthropods [for review, see Hardie (1989a), Stuart (1999), and Stuart et al. (2007)]. A role of HA and its ionotropic receptors in thermoregulation in *Drosophila* was also shown by Hong et al. (2006). In fly eyes, HA mediates synaptic transmission between photoreceptors and first-order interneurons [large monopolar cells (LMCs)], in the first visual neuropil (lamina), directly activating a postsynaptic chloride channel (Hardie, 1989b). The LMC's response is characterized by hyperpolarizing "on" and depolarizing "off" transients (Järvilehto and Zettler, 1971; Laughlin and Hardie, 1978), which can be recorded in the electroretinogram (ERG) (Heisenberg, 1971; Coombe, 1986). By screening mutants defective in these transients, Gengs et al. (2002) found that *ort* mutants had defective histamine-gated channels, and identified the *ort* gene as CG7411, also referred to as *hclA* (Gengs et al., 2002). Both *hclA* and a second histamine-gated chloride channel gene, *hclB*, were independently discovered by three groups using a bioinformatics approach (Gisselmann et al., 2002; Witte et al., 2002; Zheng et al., 2002). From their sequences, both *hclA* and *hclB* belong to the Cys-loop ligand-gated ion channel superfamily with ~40% identity to mammalian glycine receptor subunits.

Although genetic evidence clearly implicates *ort* (*hclA*), the molecular composition of the native receptor on the LMCs and in particular the role, if any, of *hclB* remain unclear. The HA dose–response (D–R) profile of the native receptor (EC_{50} = 24 μM) as well as some single-channel properties have been measured by patch clamp of dissociated *Drosophila* LMCs (Skingsley et al.,

Received April 16, 2008; revised May 29, 2008; accepted June 2, 2008.

This work was supported by the Biotechnology and Biological Sciences Research Council (R.C.H., C.-H.L.), Gatsby Charitable Trust (M.J., A.N.), the Gates Cambridge Trust (A.P.), Wellcome Trust (E.S.), and Deutsche Forschungsgemeinschaft Grants GRK1156 and SFB554 (J.R.) and Ge249/19-1 (T.R.). We are grateful to Dr. Bill Pak for contributing *hclA* and *hclB* cDNA, as well as fly stocks, and also to Drs. Jaesob Kim and Ron Davis and the Bloomington Stock Center for fly stocks. We thank Dr. Ian Meinertzhagen for helpful discussions and D. Pauls for help with cloning the enhancer fragments.

Correspondence should be addressed to Roger C. Hardie, Department of Physiology, Development, and Neuroscience, University of Cambridge, Downing Street, Cambridge CB2 3DY, UK. E-mail: rch14@cam.ac.uk.

A. Pantazis's present address: Department of Anesthesiology, University of California, Los Angeles, Los Angeles, CA 90095-7115.

J. Rister's present address: Center for Developmental Genetics, Department of Biology, New York University, 1009 Silver Center, 100 Washington Square East, New York, NY 10003.

A. S. Thum's present address: Département de Biologie/Zoologie, Université de Fribourg, Chemin du Musée 10, 1700 Fribourg, Switzerland.

DOI:10.1523/JNEUROSCI.1654-08.2008

 0270-6474/08/287250-10$15.00/0

Table 1. Previously published HA dose dependency (EC_{50} and Hill coefficient) for heterologously expressed HCLA and HCLB homomeric and heteromeric receptors, and native receptors from excised LMCs

	HCLA		HCLB		HCLA/HCLB	
	EC_{50} (μM HA)	n_H	EC_{50} (μM HA)	n_H	EC_{50} (μM HA)	n_H
Gisselmann et al. (2002, 2004)	166	1.9	10.8	1.7	2.3	1.7
Zheng et al. (2002)	14	2.7	4.2	1.6	0.87	1.3
Native (Skingsley et al., 1995)	24	2.5				
Native ort^{P306} (Gengs et al., 2002)	190	3.1				

1995; Gengs et al., 2002). When expressed in *Xenopus* oocytes, both HCLA and HCLB generated histamine-sensitive chloride currents (Gisselmann et al., 2002, 2004; Zheng et al., 2002). However, there were large discrepancies in dose–response profiles reported by these two groups (Table 1), and neither channel could be confidently matched to the properties of the native receptor, either in homomeric or heteromeric configuration. Furthermore, no single-channel properties of these novel Cys-loop receptors have yet been reported in expression studies.

In the present study, we directly compared the properties of heterologously expressed HCLA and HCLB channels with those of the native channels, and found a close match with HCLA homomers. ERG recordings confirmed that a null *ort* (*hclA*) mutation eliminated synaptic transmission. In contrast, transmission was intact in null mutants of *hclB*, but both ERGs and intracellular recordings from their LMCs revealed subtle phenotypes. Expression profiling confirmed that *hclA* was expressed in the LMCs, but *hclB* expression in the lamina was restricted exclusively to glial cells. We therefore attribute the effects of *hclB* mutation on LMC responses and the ERG to a previously unrecognized role for glial signaling in shaping the LMC response, and suggest that HCLA alone is necessary and sufficient to account for the native histamine receptors at the *Drosophila* photoreceptor–LMC synapse.

Materials and Methods

Cell transfection. Full-length *hclA* and *hclB* cDNA (provided by Dr. W. L. Pak, Purdue University, West Lafayette, IN) were subcloned into the pMT/V5-His A vector (Invitrogen), which contained a metallothionein (MT) promoter element, to produce the vectors pMT/V5-His A-hclA and pMT/V5-His A-hclB. S2 cells (Schneider, 1972) were cotransfected with a neomycin resistance plasmid, pHS-Neo, and pMT/V5-His A-hclA or pMT/V5-His A-hclB (molar ratio, 2:3) or both (ratio, 2:3:3) using Lipofectin (Invitrogen). Stable transfectants were selected by the addition of the antibiotic G418 (0.5 μg/ml; Sigma). Cells were maintained in an incubator at 25°C in nonventilated 25 cm^2 flasks (TPP) with 5 ml of full medium (Shields and Sang M3 insect medium with 0.5 g/L K_2CO_3, 12.5% fetal bovine serum, and 1% antibiotic/antimycotic solution; Sigma-Aldrich). The MT promoter was stimulated by addition of $CuSO_4$ to the culture medium (final concentration, 0.6 mM) 1–3 d before recording (Millar et al., 1995).

Electrophysiology. Cells were allowed to settle on a coverslip, which formed the floor of a Perspex chamber mounted on a Nikon Eclipse TE2000-S inverted microscope. Currents were recorded with an Axopatch 1-D amplifier and digitized and analyzed using pClamp 9 (Molecular Devices). Bath solution consisted of the following (in mM): 120 NaCl, 5 KCl, 10 *N*-Tris-(hydroxymethyl)-methyl-2-amino-ethanesulphonic acid (TES), 4 $MgCl_2$, and 1.5 $CaCl_2$. This solution was also used as vehicle for HA and in pipettes used for inside-out patches. The pipette solution for whole-cell experiments consisted of the following (in mM): 132 KCl, 10 TES, and 2 $MgCl_2$. The pH of all solutions was adjusted to 7.15 and osmolarity adjusted to 285 mOsm by D-mannitol. The junction potential using these solutions was calculated to be 4.2 mV, using Clampex 9.2, and was compensated for in calculations using holding potential. GC100F-10 borosilicate glass capillaries (Harvard Apparatus) were used for whole-cell experiments (5–10 MΩ bath resistance, series resistance <20 MΩ). Sylgard-coated and fire-polished electrodes from GC150F-7.5 capillaries were used for inside-out patches (~14 MΩ after fire polishing).

D–R experiments. Cells were whole-cell patch clamped typically at −60 mV, unless currents exceeded 1.5 nA, in which case −40 mV was used instead. A custom-made manually controlled 10-channel parallel-flow perfusion device (solution exchange rate, ~5 ms) was used for drug delivery (Skingsley et al., 1995). This system was used for consistency with the previously published results from isolated LMCs (Skingsley et al., 1995).

Control-subtracted average (or, in the case of apparent receptor desensitization, peak) current responses in every trace were normalized to the maximal current response recorded under saturating HA doses (200 μM for all receptor types) to determine the standard current, I/I_{max}. The data were fitted using the simple Hill curve:

$$\frac{I}{I_{max}} = \frac{1}{1 + \left(\frac{EC_{50}}{[HA]}\right)^{n_H}}, \quad (1)$$

where EC_{50} is the effective concentration for 50% I_{max}, and n_H is the Hill coefficient. For S2 cells cotransfected with *hclA* and *hclB*, it seemed likely that homomeric receptors were assembled, and thus contributed to the observed current, along with any heteromers. Therefore, data from cotransfected cells were also fitted with a composite Hill equation:

$$\frac{I}{I_{max}} = \frac{w_{HCLA}}{1 + \left(\frac{EC_{50HCLA}}{[HA]}\right)^{n_{HCLA}}} + \frac{w_{HCLB}}{1 + \left(\frac{EC_{50HCLB}}{[HA]}\right)^{n_{HCLB}}} + \frac{1 - (w_{HCLA} + w_{HCLB})}{1 + \left(\frac{EC_{50hetero}}{[HA]}\right)^{n_{hetero}}}, \quad (2)$$

where w represents the proportion of the current contributed by each receptor type.

Noise analysis. Macroscopic current noise can yield information about the underlying single-channel currents, assuming the noise is generated by the stochastic opening and shutting of the channels (Colquhoun and Hawkes, 1977). Five-second steady-state current recordings were taken from cells clamped at −80 mV, with or without histamine at concentrations below the EC_{20}. Cell capacitance (C) and series resistance (R_s) were not compensated, but a 100 ms, +10 mV square pulse was used to measure the clamp time constant ($\tau_{RC} = R_s \times C$), to later correct for the RC filtering and variance underestimation.

After measuring the mean current amplitude the traces were baseline adjusted and filtered off-line by a 10 Hz high-pass Bessel (eight-pole) filter (Clampfit 9.2) before measuring the variance. Clampfit was also used to extract power spectra by fast Fourier transform using a Blackman window and averaged overlapping recording sections of 1024 points each. The spectra for the HA and control current traces were compensated for τ_{RC} before the control was subtracted. The resulting spectrum was subsequently fitted with single or double Lorentzian functions, from 20 Hz until the spectrum became too noisy, typically 2–3 kHz. The fitted time constants were used as indicators of single-channel kinetics and also

to estimate the variance underestimation resulting from the clamp time constant.

Single-channel recording, acquisition and analysis. Single channels were recorded and analyzed from excised inside-out patches. Preliminary analysis revealed that they did not obviously differ from those from cell-attached recordings. The signal was prefiltered by the amplifier with a low-pass $f_c = 10$ kHz (−3 dB) and then digitized at $f_s = 100$ kHz. Records were further filtered with the software Gaussian filter in Clampfit 9.2 to $f_c = 2$ kHz, and decimated to a sample frequency of 20 kHz. The combined f_c of the amplifier prefiltering and software filtering on the records was 1.9 kHz.

Records were idealized using the SCAN idealization software. Over 5000 transitions were fitted from each trace. A 100 μs temporal resolution (t_{res}) was imposed on the idealized record. Amplitude and dwell time distributions were generated and fitted by maximum likelihood using EKDIST. Both SCAN and EKDIST are parts of the DCPROGS single-channel analysis suite by Colquhoun and Vais (http://www.ucl.ac.uk/pharmacology/dc.html).

Single-channel records from dissociated LMCs had been previously recorded on a digital tape recorder at 20 kHz sampling rate by Skingsley et al. (1995) and filtered by a 2 kHz Bessel filter. They were redigitized and analyzed in the same way as the traces from S2 cells, using DC-PROGS.

In vivo *intracellular LMC recordings.* Flies were immobilized within a brass fly holder (Juusola and Hardie, 2001; Zheng et al., 2006), and intracellular voltage responses of LMCs were recorded using sharp borosilicate microelectrodes (Sutter Instruments) of resistance 120–200 MΩ inserted through a small hole cut in the cornea. The electrode solution was 3 M K-acetate with 0.5 mM KCl to sustain the LMCs' chloride battery (Hardie, 1989b). The head temperature of the flies was kept at 19 ± 0.5°C by a feedback-controlled Peltier device (Juusola and Hardie, 2001). LMCs were stimulated by 10 ms light pulses from four high-intensity green light-emitting diodes (Marl Optosource; peak emission, 525 nm), delivered by a randomized fiber optic bundle. This light guide was mounted on a Cardan arm system, enabling free positioning of the light source with equal distance to the eye. The light source, which subtended 5° as seen by the fly, was positioned at the center of a LMC's receptive field. Intensity was controlled by neutral density filters (Kodak) covering a range of 6 log units from ~6 to ~6×10^6 effectively absorbed photons/s/photoreceptor. The LMCs were first tested with dim pulses before increasing the intensity. Responses were amplified by SEC-10L (NPI Electronic) in current-clamp mode using ~15 kHz switching rate, low-pass filtered at 1.5 kHz (Kemo VBF8), and sampled at 10 kHz. Stimulus generation and data acquisition were performed by custom-written software: BIOSYST (Juusola and Hardie, 2001).

ERGs. For ERG recordings, flies were immobilized within the cut ends of Eppendorf tips with a drop of low-melting-point wax and recorded using patch pipettes filled with bath solution (see above) positioned in a drop of conducting gel on the surface of the eye. The indifferent electrode contacted the head carapace again via conducting gel. Signals were amplified via a DAM60 differential DC amplifier (World Precision Instruments) and sampled and recorded using Clampex 6.0 software. Illumination was via a DC-regulated 50 W halogen lamp filtered with a Schott OG560 cutoff filter (orange) and Wratten neutral density filters covering 6 log units (maximum intensity equivalent to ~5×10^6 effectively absorbed photons/s/photoreceptor). Light was delivered via a liquid light guide (5 mm diameter) positioned 5 mm from the eye, and controlled via a Uniblitz electronic shutter (Vincent Associates).

Cloning of the histamine receptor enhancer fragments. Genomic enhancer DNA was amplified from wild-type Canton-S flies with the TripleMaster PCR system (Eppendorf). For the *ort* (*hclA*)-GAL4 construct, a 3126 bp fragment from the 5′ *ort* (*hclA*) enhancer region was amplified using the primers 5′-GAGAGCGGCCGCGCGGCTA-CAGGTTTGTTTGT-3′ and 5′-GAGAGGTACCAGTTGGTGGCG-AACAGATTT-3′. For the *hclB*-GAL4 construct, a 4654 bp fragment from the 5′ *hclB* enhancer region was amplified using the primers 5′-GAGAGCGGCCGCCACTGGCTGATTGCAAAAG-3′ and 5′-GAGAG-GTACCATTCGCTTTCATTGGCATTC-3′. After subcloning into pBluescript using *Not*I and *Kpn*I, the promoter fragments were cut by *Kpn*I and *Not*I and cloned into pPTGAL for germline transformation (Sharma et al., 2002). *Drosophila* germline transformation was performed by a standard procedure using the plasmid pπ25.7 Δ2–3 wc (Spradling and Rubin, 1982) as a source of transposase. Several independent insertions of *ort* (*hclA*)-GAL4 and *hclB*-Gal4 were created. Because reporter expression was weaker and patchy in single-insertion strains, second and third chromosomal insertions were combined to increase the GAL4 expression level.

Immunohistochemistry. Vibratome sections and immunohistochemistry were performed as described previously (Rister et al., 2007). Briefly, female flies were fixed in 4% paraformaldehyde in PBS overnight at 4°C. Next, they were embedded in hot ($T = 65$°C) 8% agarose, and horizontal head sections were cut with a vibratome (Leica). The sections were washed five times for 20 min each in PBST (PBS containing 0.5% Triton X-100; Sigma) and then blocked for 1 h with normal goat serum (Dianova) in PBST. Sections were incubated overnight at 4°C with polyclonal rabbit anti-green fluorescent protein (GFP) antiserum (1:1000; Invitrogen) or rabbit anti-β-Gal (1:1000; Invitrogen). As secondary antibody, goat anti-rabbit IgG Alexa Fluor 488 conjugated (Fab′) fragment of IgG (1:100; Invitrogen) or goat anti-rabbit CY3 (1:100; Invitrogen) was used. Three-dimensional image stacks were collected with a 40× or a 63× oil objective at 0.8 μm steps with a Leica confocal microscope and further processed using the software Amira (Mercury Computer Systems).

Expression profiling by mRNA tagging. Expression profiling was performed with whole brains (including optic lobes and lamina) dissected from Canton-S flies. RNA was isolated with trizol and used for cDNA synthesis with the superscript III reverse transcriptase (Invitrogen). After purification, the cDNA served as template for conventional PCR with oligonucleotides derived from the coding regions of the following genes: *rpl32*, *elav*, *repo*, *hclA*, and *hclB*. PCR was performed for 30 cycles, and equal aliquots were loaded onto a 2% agarose gel. The no-template control was treated exactly as the *rpl32* sample, except that no reverse transcriptase was added to the reaction. For mRNA-tagging experiments, we crossed each of three Gal4 driver lines: *elav-Gal4* (neuronal expression), *repo-Gal4* (expression in glia), and *L2-Gal4* [expression in LMCs (Rister et al., 2007)] with a UAS-line carrying the FLAG-tagged human poly(A)-binding protein (PABP) gene [*UAS-hPF* (Yang et al., 2005)]. The mRNA-tagging procedure was performed essentially as described previously (Yang et al., 2005) with only minor modifications. Animals were kept at 18°C. We isolated the brains of ~50 young adults from the corresponding crosses manually. In contrast to the original protocol, we used anti-Flag-M2-biotin conjugates (Sigma-Aldrich) bound to streptavidin-coupled magnetic beads. After elution of the mRNA, we amplified the entire mRNA population using a capfinder approach essentially as described previously (Franz et al., 1999). Amplified and purified material was used as template for conventional PCR experiments (see above).

Flies. Flies used for ERG recordings included w^{1118};;ort^{US6096}, a null mutant for the *ort* (*hclA*) gene in which nucleotides 359–361 (CCA) are replaced with AG resulting in a frameshift (Gengs et al., 2002), and w^{1118};; $hisCl1^{134}$, a null mutation in the *hclB* gene encoding the second histamine-gated chloride channel. $hisCl1^{134}$ was generated by imprecise P-element excision deleting 1.7 kb of the gene including the region coding for the ligand-binding domain and three transmembrane segments (Hong et al., 2006). "Wild-type" controls were performed using white-eyed flies (w^{1118}).

The following UAS reporter and Gal4-driver stocks were obtained from the Bloomington Stock Center: cytoplasmic GFP (*UAS-GFP*), membrane-associated GFP (*UAS-mCD8-GFP*), and nuclear-localized lacZ (*UAS-nlslacZ*); *repo-Gal4* (glia) and *elav*-Gal4 (neurons).

Nomenclature. Because of the independent discovery of these novel channels, different nomenclatures exist in the literature. The nomenclature used in this paper (*ort* = *hclA*, and *hclB* for genes, and HCLA and HCLB for their protein products, respectively) is the same used by Gengs et al. (2002). *ort* (*hclA*) has also been referred to as *hisCl2* (Zheng et al., 2002) and *HisCl-*α1 (Gisselmann et al., 2002) with *hclB* being cited as *hisCl1* and *HisCl-*α2 by the same respective authors.

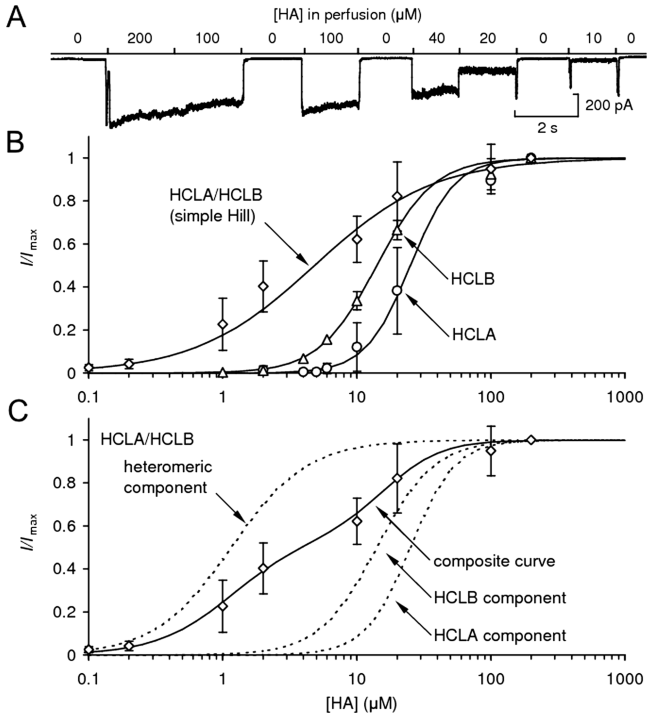

Figure 1. Dose–response functions of HCLA and HCLB channels. ***A***, Current recorded from an S2 cell transfected with *hclA*, whole-cell patch clamped at −60 mV. HA was applied using a 10-channel parallel-flow drug delivery system (Skingsley et al., 1995) at the concentrations indicated. ***B***, Simple Hill fittings for data from cells transfected with *hclA* (circles), *hclB* (triangles), or both (diamonds). ***C***, Composite Hill curve [Hill equation with weighted components for the contributions of different receptor types (Eq. 2)]; fits for data from cotransfected cells (diamonds and solid curve), as well as the individual components of the equation (dashed curves), are shown. Error bars represent ±1 SD.

Results

Dose–response experiments

As previously reported (Hardie et al., 1997), S2 cells can be routinely patch clamped in both whole-cell configuration and excised patch mode. Twenty-four hours after stimulation of the MT promoter by 0.6 mM Cu^{2+}, large whole-cell currents could be elicited by HA application: typically ~0.5 nA for *hclB* and *hclA*/*hclB* (cotransfected) cells, and up to a few nanoamperes for *hclA*-transfected cells at −60 mV holding potential and saturating agonist concentration. The larger currents in *hclA*-expressing cells likely reflect the larger single-channel conductance of the HCLA channel (see below). In all cells, slow desensitization ($\tau > 200$ ms) was evident when concentrations above the EC_{50} were applied.

Figure 1*A* shows a typical dose–response experiment on an S2 cell transfected with *hclA*. Figure 1*B* shows the simple Hill curve fittings (Eq. 1) of the data from all D–R experiments from singly transfected (HCLA and HCLB) and cotransfected (HCLA/HCLB) cells. Fitted parameters are shown in Table 2.

In contrast to previous studies (Table 1), in which *hclA* was expressed in *Xenopus* oocytes (Gisselmann et al., 2002, 2004; Zheng et al., 2002), we found an almost exact match between the dose–response characteristics of HCLA homomeric receptors and the native LMC receptor (Skingsley et al., 1995), both in terms of EC_{50} (24 vs 25 μM) and cooperativity (n_H = 2.5 vs 2.6). Neither parameter (EC_{50} or n_H) recorded in S2 cells was statistically different from the respective value for the native receptor in LMC (Student's *t* test). Cells expressing HCLB receptors alone were slightly (1.7 times) more sensitive to HA than the native receptors or cells expressing HCLA and had a shallower slope (n_H = 2.0). Although statistically significant ($p < 0.05$), these relatively minor differences alone would be insufficient to exclude the possibility that the native receptors might be composed at least partially of HCLB homomers.

In contrast, it was evident, both from single and composite Hill fittings of data from cotransfected cells, that HCLA and HCLB subunits formed functional heteromeric receptors, which were significantly more sensitive to histamine (EC_{50} = 4.8 μM). This agrees with previous studies, which also concluded the existence of heteromers on the basis of increased cotransfectant sensitivity (Zheng et al., 2002; Gisselmann et al., 2004). The large difference between the EC_{50} values of cotransfectant S2 cells and isolated LMCs implied that heteromers did not significantly contribute to the HA-dependent currents recorded from LMCs.

The EC_{50} for cotransfected cells was estimated at 4.8 μM using a single Hill equation (Eq. 1); however, the D–R function had a shallow and irregular slope, and it seemed possible that the conductance was generated by channels with a range of subunit compositions, including both HCLA/B heteromers and HCLA and HCLB homomers. The data were therefore also fitted using a composite Hill equation (Eq. 2, Materials and Methods) fixing the separately derived EC_{50} and n_H values for the homomeric channels, leaving n_H and EC_{50} of the heteromeric component and relative weightings as free parameters (Fig. 1*C*). This generated a better fit to the D–R function and yielded an EC_{50} value of 1.2 μM and n_H of 1.5 for the heteromeric component, which, from the fitting procedure, was estimated to account for ~55% of the current. Because the receptor is likely to be a pentameric assembly, even this component could of course be composed of different channels with distinct heteromeric subunit stoichiometries.

Noise analysis experiments

Because there was no previously published information on the single-channel properties of heterologously expressed HCLA or HCLB channels, we first characterized their properties by noise analysis. Analysis was performed with concentrations at or below the EC_{20}, where the amplitude-variance parabola can be reasonably approximated by a straight line. Figure 2 shows a typical current fluctuation experiment on an *hclA*-transfected S2 cell at a holding potential of −60 mV. The results of this analysis on all transfected cells are shown in Table 3.

Lorentzian functions fitted to the power spectra of the noise indicated that the kinetics for all receptor types were in the near-millisecond and submillisecond range. Effective single-channel current amplitudes were estimated from the variance/mean current ratio and corrected for filtering of the noise by the clamp time constant (see Materials and Methods). This indicated that both HCLB homomers and heteromeric HCLA/HCLB receptors had rather low effective single-channel conductance (~4 pS). In contrast, the estimated single-channel conductance for HCLA homomers was an order of magnitude larger, ~45 pS.

Skingsley et al. (1995) reported a single-channel conductance of 58 pS for the native receptors. This is very distinct from estimated values for HCLB homomers and heteromeric receptors, but close to the 45 pS value estimated for HCLA homomers. Although the correspondence is not sufficiently close to argue for functional equivalence, the fact that HCLA homomers have such a high conductance suggested that a more detailed direct single-channel analysis could be successfully performed. HCLB homomers and heteromeric receptors were not investigated further at the single-channel level, because their low predicted conductances would make single-channel analysis impractical and were in any case clearly distinct from the native receptor.

Single-channel analysis

Channel activity was reliably detected in the majority of cell-attached or excised inside-out patches from HCLA-expressing S2 cells, using electrodes containing 10 μM HA. Single-channel traces from excised inside-out patches of both HCLA homomeric receptors and native HA receptors from dissociated LMCs were analyzed in terms of their conductance and open time distributions, at positive and negative holding potentials. Samples of the traces and the distributions are shown in Figure 3, and the fitting parameters for the latter are listed in Table 4.

In both HCLA traces, clusters of activations (i.e., bursts of activations separated by shut intervals where the receptor is presumed to be unbound) were discernible, separated by longer intervals of presumed receptor desensitization. At negative-holding potentials, the open probability within these clusters (P_{open}, defined as the open duration divided by the total cluster duration) was 0.16 ± 0.02 (12 clusters), in agreement with the macroscopic current expected to be elicited by this concentration (14% of I_{max} according to the D–R curve). At lower agonist concentration, individual clusters were no longer discernible, probably because the closed intervals attributable to unbound receptor were of similar duration to the dwell times of desensitized states (data not shown).

At negative holding potentials (−80 mV), the amplitude distribution of HCLA channels revealed three distinct conductance levels at ~25, 45, and 60 pS, each accounting for ~20–60% of the area. At positive holding potentials, however, the largest conductance level appeared to be absent, leaving only 25 pS (~35%) and 40 pS (~65%) subconductance states. The conductance determined by current fluctuation analysis (45 pS) would have been the weighted average of these distinct conductance levels, and therefore fully consistent with the direct single-channel analysis.

Analysis of the native receptor channels revealed an almost identical behavior. Specifically, we could again identify three similarly sized and weighted conductance levels at −80 mV. Strikingly, the largest conductance level was again absent at positive (+80 mV) potentials. In terms of kinetics, both receptors also appeared to have similar submillisecond and near-millisecond openings (Fig. 3, Table 4). Although the derived open times were not perfectly matched, this may have reflected the lower bandwidth and somewhat inferior signal-to-noise ratio of recordings from the native channels, which would, e.g., have resulted in more missed brief events.

Table 2. Histamine dose–response parameters

Receptor type	EC_{50} (μM HA)	n_H	*n* (cells)
HCLA homomers	25.0 ± 8.8	2.6 ± 0.6	9
HCLB homomers	14.1 ± 1.7	2.0 ± 0.4	6
HCLA/HCLB[a]	4.8 ± 2.6	1.0 ± 0.2	9
HCLA/HCLB[b]	1.2	1.5	9
Native[c]	24.0 ± 8.5	2.5 ± 0.5	27

All fitted parameters are mean ± 1 SD.

[a]Simple Hill equation fitting parameters (see Eq. 1, Fig. 2*A*).

[b]Heteromeric component parameters of the composite Hill equation (see Materials and Methods, Eq. 2, and Fig. 2*B*).

[c]Data from Skingsley et al. (1995).

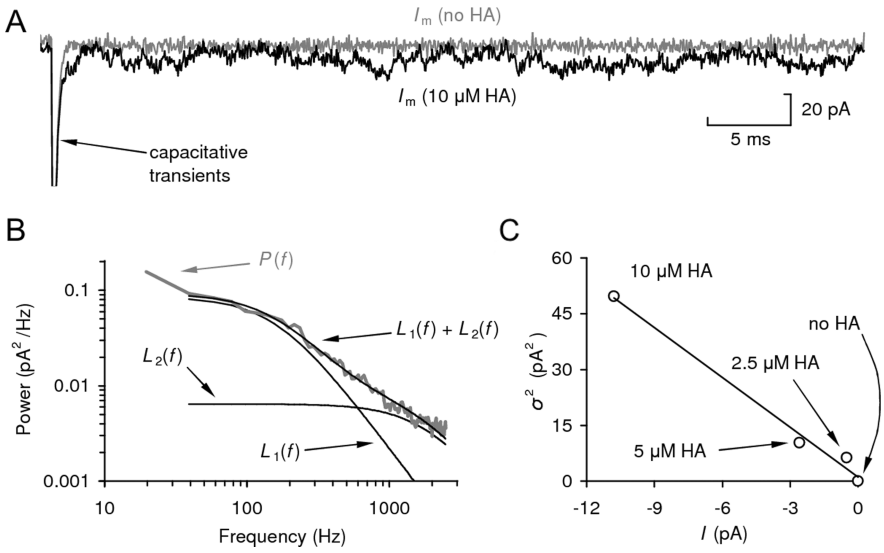

Figure 2. A typical noise analysis experiment. ***A***, Whole-cell patch-clamp recording from an S2 cell transfected with *hclA*, held at −80 mV. Current was recorded in the presence (10 μM) and absence of HA. The capacitative transients generated by a +10 mV pulse were used to determine the clamp time constant, τ_{RC} (180 μs). ***B***, Power spectrum (*P*) for channel noise at 10 μM HA, fitted with a double Lorentzian function. The component Lorentzian curves, L_1 and L_2, are also plotted (time constants, $\tau_1 = 0.08 \pm 0.01$ ms and $\tau_2 = 0.98 \pm 0.03$ ms, with normalized weights $w_1 = 0.07 \pm 0.01$ and $w_2 = 0.93 \pm 0.01$). The correction factor to compensate the variance was calculated to be 1.71. ***C***, Plot of macroscopic current variance (σ^2) against control-subtracted average current (*I*) at three different HA concentrations and without HA. The slope of the linear regression, hence single-channel current, was −4.47 pA ($R^2 = 0.99$), indicating a single-channel conductance (γ) of 55.9 pS (at −80 mV).

Effects of *hclB* and *ort* (*hclA*) mutations on synaptic transmission

The close congruence of D–R functions as well as single-channel properties found between the native LMC histamine-gated chloride channel and heterologously expressed HCLA suggests that the native channels are composed of HCLA homomeric channels. As an independent test for the contribution of HCLA and HCLB to synaptic transmission, we also recorded ERGs from mutants of both channels. In wild-type flies, the ERG is characterized by a corneal negative sustained photoreceptor component with brief depolarizing "on" and negative "off" transients (Fig. 4), which are primarily derived from the LMC response (Heisenberg, 1971; Coombe, 1986; Buchner, 1991). Previously, ERG transients were reported to be lacking in a variety of *hclA* (*ort*) alleles (O'Tousa et al., 1989; Gengs et al., 2002; Rajaram et al., 2005). However, in at least one of these alleles (ort^{P306}), small transients can in fact be detected with bright stimulation, and substantial synaptic transmission to the LMCs in this mutant was confirmed by intracellular recordings (Zheng et al., 2006). We therefore reinvestigated an alternative, genuine null *ort* allele (ort^{US6096}), which has a frame shift in the ORF, before the transmembrane helices (Gengs et al., 2002), and is therefore incapable of making functional channels. Although we confirmed the presence of residual transients in ort^{P306} (data not shown), in ort^{US6096} there was never the slightest indication of a positive "on" or negative "off" transient, even at saturating intensities. Instead, as in other synaptic mutants, at light on, bright flashes elicited a negative going peak transient, which is interpreted as the peak-to-

Table 3. Current fluctuation analysis results

Transfection	γ (pS)	τ_1 (ms)	τ_2 (ms)	w_2/w_1	*n* (cells)
hclA	44.8 ± 9.5	0.20 ± 0.13	1.0 ± 0.2	34.2	7
hclB	4.2 ± 2.0	0.41 ± 0.18	6.1 ± 1.0	5.8	4
hclA and *hclB*	4.0 ± 1.5	0.28 ± 0.14	3.7 ± 1.7	14.1	6

γ, Effective single conductance; t_1 and t_2, Lorentzian time constants; w_2/w_1, relative weighting.

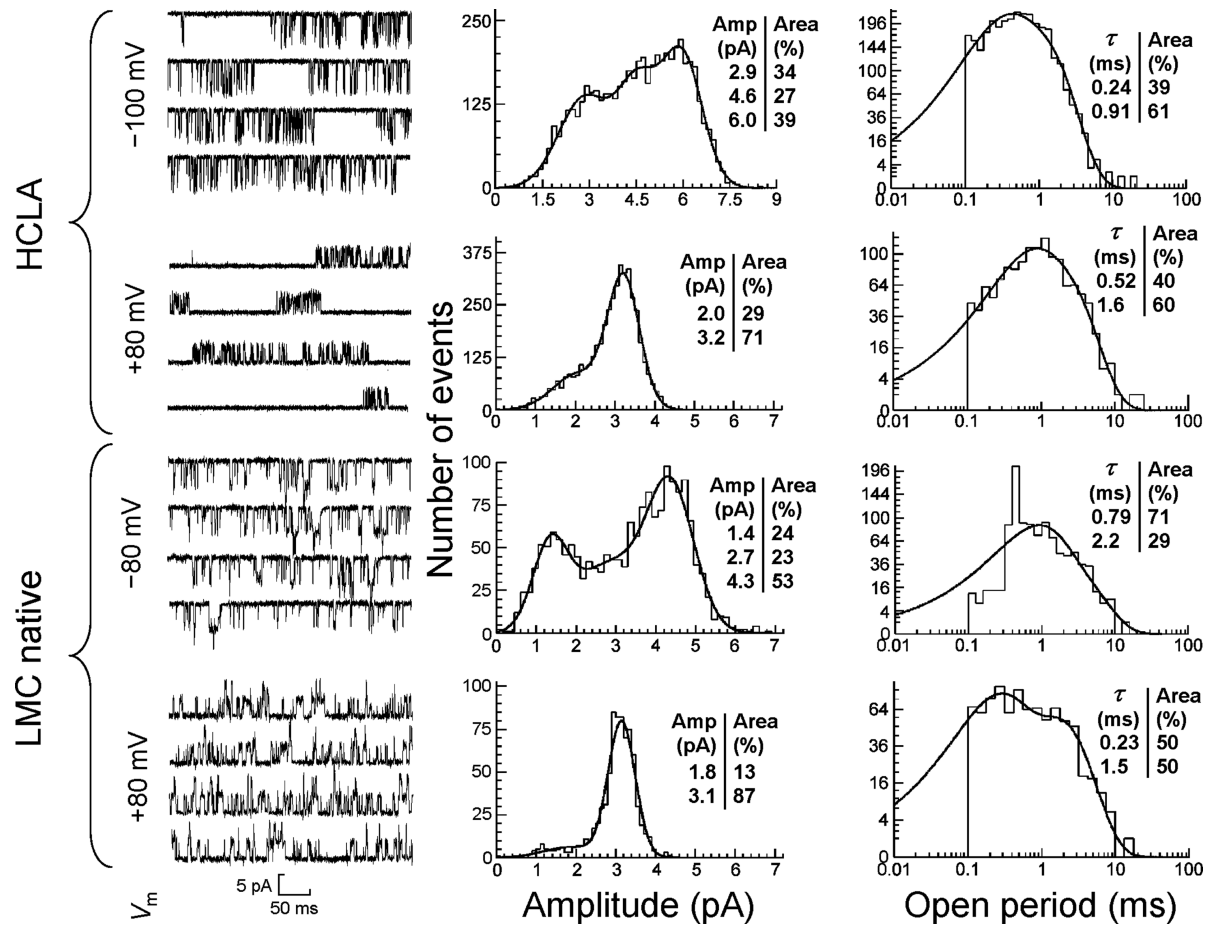

Figure 3. Single-channel properties of HCLA channels. Left, Sample single-channel recordings from HCLA homomers (from *hclA*-transfected S2 cells) and native HA receptors (from *Drosophila* LMCs), recorded at the holding potentials indicated, with 10 μM HA in the recording pipette in both cases. At least 5000 transitions from each recording were idealized with SCAN. Middle, Amplitude (Amp) distributions of time course-fitted opening transitions, generated and fitted with multiple Gaussians by maximum likelihood with EKDIST (fitted amplitudes and relative contributions of subconductance states are indicated). Right, Open time distributions of fitted transitions, generated and fitted by multiple exponentials with EKDIST. Fitted time constants and relative contributions are indicated in insets. A 100 μs time resolution was imposed for all distributions.

plateau transition of the photoreceptor component that is normally superimposed on the synaptic transients (Fig. 4).

In addition we recorded from a null allele of the *hclB* gene, *hisCl1*^{134} (Hong et al., 2006), which has a 1.7 kb deletion including the ligand-binding domain and three transmembrane regions. In marked contrast to *ort* mutants, robust "on" and "off" transients were invariably recorded in *hisCl1*^{134} mutants, and the "off" transients were very similar to wild type. Although the "on" transients were qualitatively also very similar to wild type, surprisingly the maximum amplitudes were actually approximately twofold larger (Fig. 4).

As a more direct measure of synaptic

Table 4. Single-channel characteristics (conductance levels and relative areas) for recombinant HCLA homomers and native HA receptors from LMCs at different holding potentials

Receptor	V_m (mV)	γ (pS)	*A* (%)
HCLA homomeric	−100[a]	25.9 ± 8.4	20
		43.9 ± 6.4	21
		59.9 ± 6.5	59
	+80[b]	24.9 ± 10.0	35
		39.2 ± 4.2	65
LMC native	−80	16.8 ± 5.5	21
		35.5 ± 10.6	32
		54.6 ± 7.4	47
	+80	23.0 ± 8.1	13
		39.3 ± 4.3	87

The data from the native receptor are based on a single exemplary recording (10 μM HA). Data from five further native patches showed similar behavior with a major conductance state of 50–60 pS at −80 mV and clear indications of subconductance states, but recording quality was not suitable for more rigorous analysis. Data are based on >1500 channel transitions per patch (after imposition of 100 μs resolution). γ, Conductance levels; *A*, relative areas; V_m, holding potential. [a]$n = 4$ patches. [b]$n = 2$ patches.

transmission, we also made intracellular recordings from the LMCs in *hisCl1*^{134} mutants. Recordings from LMCs in both wild-type (*w*^{1118}) controls and *hisCl1*^{134} were characterized by similar resting potentials (wild type, −43 ± 7.3 mV vs *hisCl1*, −45 ± 12.7 mV; $n = 6$). Both also responded to brief flashes of increasing intensity with graded transient hyperpolarizations as previously described in wild-type red-eyed *Drosophila* (Zheng et al., 2006). As in the ERG recordings, however, subtle differences were noted; although maximum responses were of similar amplitude (−15 to −25 mV) and elicited at similar intensities, the rise time of the response waveforms in *hisCl1*^{134} mutants was significantly (approximately twofold) slower than in the wild-type controls with times to peak delayed by ~10–20 ms. The *hisCl1*^{134} mutant responses were also slightly less sensitive to low intensity flashes so that the resulting *V*/log *I* function was significantly steeper (Fig. 5).

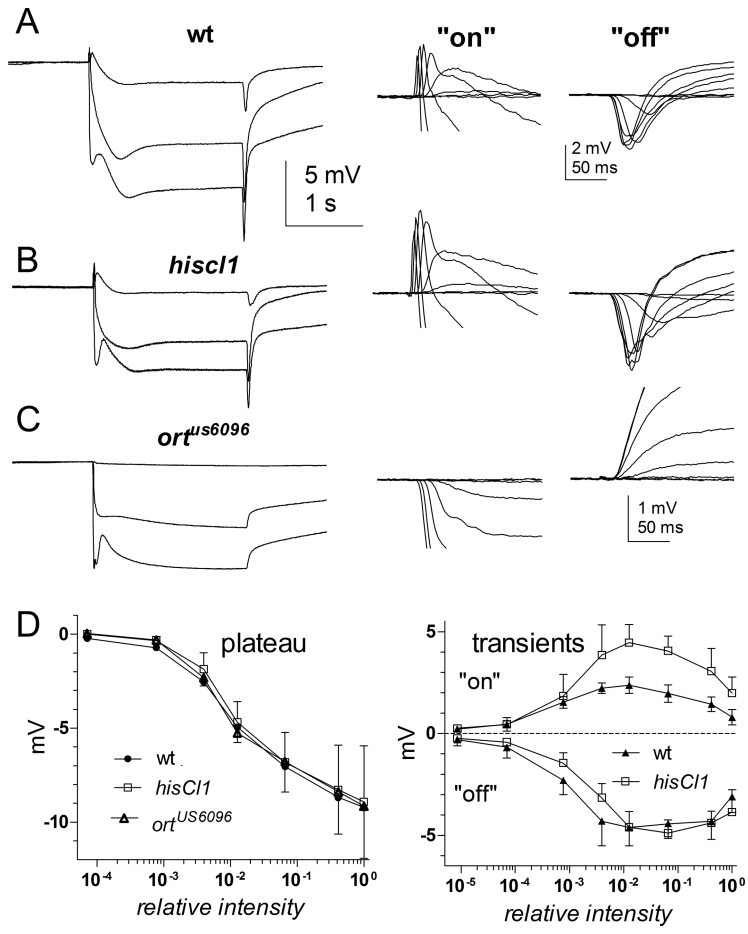

Figure 4. ERGs from *hclA* (*ort*) and *hclB* (*hisCl1*) mutants. ***A***, ERGs recorded in response to 2 s light steps of increasing intensity in wild-type (wt; i. e., *w*^{1118}) control flies. The conspicuous transients at light on and off represent the contribution of the LMCs in the lamina. ***B***, ***C***, ERGs recorded using identical stimulation in a null *hclB* mutant (*w*^{1118};;*hisCl1*^{134}; ***B***) and a null *hclA* mutant (*w*^{1118};;*ort*^{US6096}; ***C***). Examples of "on" (left) and "off" (right) transients in response to increasing intensities (7 steps covering 6 log units of intensity) are shown on the right on an expanded scale after aligning baselines immediately before light on or off. Transients were completely eliminated in *ort* null (note larger scale). Transients in *hisCl1*^{134} were qualitatively similar in waveform to wild-type controls, but the "on" transients were approximately twofold larger. ***D***, Response intensity functions for the maintained negative plateau (photoreceptor component) in wild type (wt; *w*^{1118}), *ort*^{US6096}, and *hisCl1*^{134} (left); and both "on" and "off" transients in wt and *hisCl1*^{134} (right). Data (mean ± SD) are based on ERGs from $n = 5$–6 flies for each genotype.

Expression profiles of HCLA and HCLB

The differences in LMC and ERG responses in *hclB* mutants might suggest that, after all, HCLB subunits also contribute to the synaptic receptor on the LMCs. To investigate this further, we investigated the expression profile of the two *hcl* genes, and in particular asked whether the *hclB* gene is expressed in the LMCs. Previous data using *in situ* hybridization or antibody staining are equivocal on this point, and have lacked good cellular resolution (see Discussion). We investigated *hclA* and *hclB* expression using two independent approaches. First we used a reporter gene strategy, using upstream enhancer elements of the two *hcl* genes to drive expression of GFP and lacZ (Fig. 6*A–D*). As expected, the *hclA* enhancer (Fig. 6*D*) drove GFP expression in LMCs L1–L3 (Fig. 6*A*), as well as cells closely resembling amacrine cells (data not shown). The large LMC cell bodies in the lamina cell body layer, along with their radially oriented dendrites in the lamina neuropil, were immunopositive for GFP. In the medulla, the characteristic terminals of L1, L2, and L3 were stained in layers M1, M2, M3, and M5 (Fig. 6*A*, inset; arrowhead indicates L3 terminal layer). The medulla rind exhibited staining of cell bodies (Fig. 6*A*, cb) of transmedullary cells. Their columnar axons and distal stratifications (Fig. 6*A*, open arrowhead) were labeled in the medulla, as well as their terminals in the lobula (data not shown). These cell types were not studied further, but are most likely the targets of photoreceptors R7 and R8.

In contrast, an extensive 5′ enhancer region of the *hclB* gene fused to GAL4 drove expression in a very different pattern in the lamina (Fig. 6*B–D*). There was clearly no indication of expression in the LMCs (Fig. 6*B*, cartridge cross section). Interestingly, however, strong and exclusive expression was detected in the lamina epithelial glia cells that surround the lamina cartridges (Fig. 6*B*, inset) and have their cell bodies distal in the lamina neuropil (Fig. 6*C*). This latter feature distinguishes them from amacrine cells, which are the only other intrinsic cells in the lamina and which have proximally located cell bodies (Strausfeld and Nässel, 1980). It has long been known that the lamina glia cells receive direct synaptic input from the R1–R6 photoreceptors (Burkhardt and Braitenberg, 1976; Nicol and Meinertzhagen, 1982; Shaw, 1984; Meinertzhagen and O'Neil, 1991), but the significance of this synapse has remained mysterious.

In a second approach, we implemented a recently developed mRNA tagging technique (Yang et al., 2005) to determine expression of both *hclA* and *hclB* in the LMCs and glia. We first performed conventional reverse transcription (RT)-PCR of complete brains of adult flies and confirmed that both *hcl* genes as well as the neuronal (*elav*), glial (*repo*), and general housekeeping controls (*rpl32*) are expressed in this preparation (Fig. 7). To isolate mRNA from specific cell types, we then used the UAS-Gal4 system to drive expression of a FLAG-tagged human poly(A)-binding protein (PABP) in specific cell types only (Yang et al., 2005), namely, all neurons (*elav-Gal4*), glia (*repo-Gal4*), and LMCs (*L2-Gal4*). After immunoprecipitation of the PABP-mRNA complexes, the mRNA was eluted and amplified by RT-

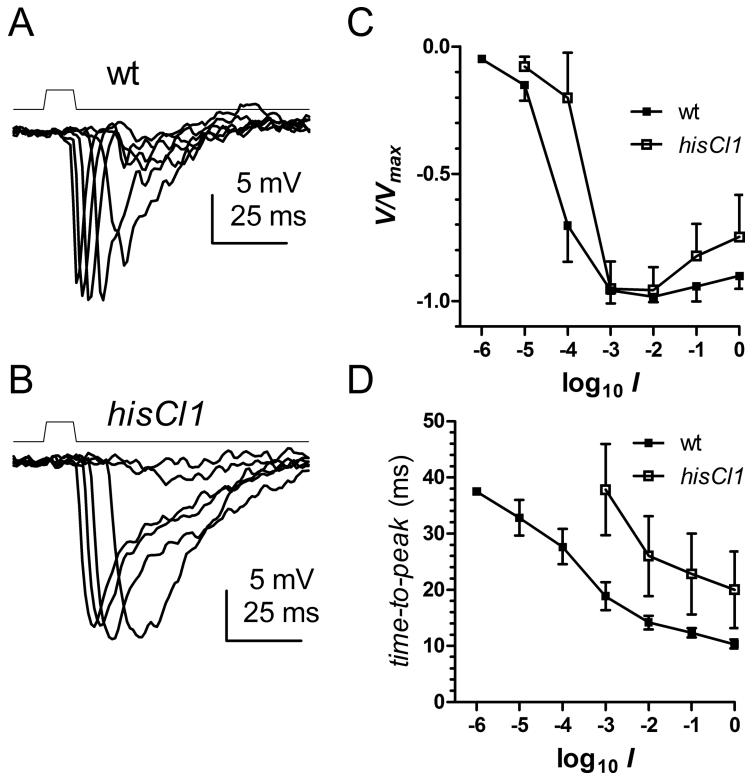

Figure 5. Intracellular LMC recordings from wild-type (wt; w^{1118}) and *hclB* ($hisCl1^{134}$) mutants. ***A***, ***B***, Responses to brief (10 ms) flashes of increasing intensity ($\log_{10}$ steps) in wild-type (w^{1118}; ***A***) and w^{1118};;$hisCl1^{134}$ mutants (***B***). ***C***, Averaged, normalized response intensity ($V/\log I$) functions in wild-type (w^{1118}) and w^{1118};;$hisCl1^{134}$ mutants. ***D***, Averaged time to peak at different intensities (mean ± SD; $n = 6$ cells).

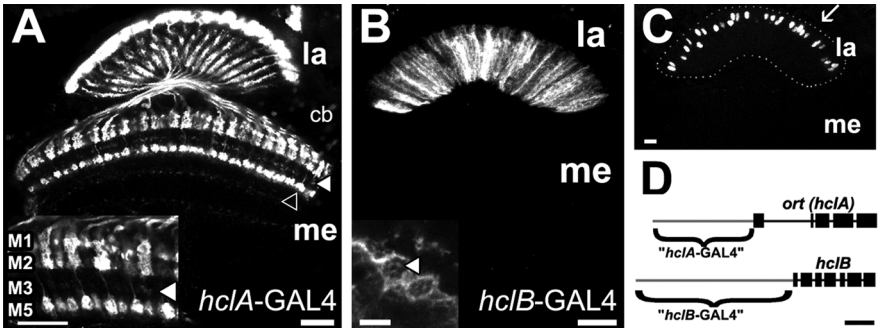

Figure 6. Enhancer analysis of the two histamine receptor genes. ***A***, *ort* (*hclA*)-GAL4-driven expression of GFP. The reporter was detected in lamina (la) monopolar cells L1–L3 (see also inset) and medulla (me) cells (indicated by open arrowhead). cb, Cell bodies. The L3 terminal layer is indicated by a filled arrowhead. The inset shows a 40× magnification of the distal medulla. Layers M1, M2, M3, and M5 were immunopositive, corresponding to the specializations of L1 (M1 and M5), as well as the terminals of L2 (M2) and L3 (M3, indicated by filled arrowhead). Scale bars, 20 μm. ***B***, *hclB*-GAL4-driven GFP expression. Intrinsic cells in the lamina, but not the monopolar cells, were labeled by this line (compare with ***A***). Scale bar, 20 μm. Inset, Cartridge cross sections reveal that the fibers are epithelial glia that surround the neuroommatidia. Note that the axon terminals of R1–R6 are also not stained (one indicated by arrowhead). Scale bar, 5 μm. ***C***, The same driver as in ***B*** combined with a nuclear-localized lacZ reporter. The cell bodies of the immunopositive epithelial glia are within the lamina neuropil (outline indicated by dots), not in the cell body layer, which is located more distally (arrow). Scale bar, 20 μm. ***D***, Schematic of the genomic structure of the two histamine receptor genes *hclA* and *hclB*. Light gray lines indicate enhancer regions that were used for expression of GAL4. Scale bar, 1 kb.

PCR using primers for *hclA* and *hclB* to identify the expression profiles of the two *hcl* genes (Fig. 7). In confirmation of our results using reporter genes, only *hclB* was detected in glial cells. Furthermore, whereas both genes were expressed in neurons in general (*elav4-Gal4*), in the LMC preparation (*L2-Gal4*), only *hclA*, not the *hclB* gene, was expressed (Fig. 7). The corresponding controls using primers for *elav* and *repo* revealed that the preparations were devoid of contaminating material.

In summary, two independent approaches provide complementary and compelling evidence that, within the lamina, *hclB* is expressed exclusively in the epithelial glia, whereas *hclA* is expressed in the LMCs and probably also amacrine cells. These results are thus fully consistent with the proposal that the native LMC receptor is an HCLA homomer. We propose that the subtle effects of the $hisCl1^{134}$ mutant on ERG transients and LMC response are an indirect consequence of a defect in signaling between R1–R6 and the lamina glia using HCLB channels.

Discussion

We have compared the properties of recombinant HCLA and HCLB channels with those of the native channels, recorded ERGs from null mutants in both genes, made intracellular recordings from LMCs in wild-type and *hclB* mutants, and determined the expression profile of the *hclB* and *hclA* genes. As well as addressing the molecular identity of the native receptor on the LMCs, our results provide the first single-channel analysis of this new family of Cys-loop ligand-gated ion channel (LGIC) and reveal a novel role for the lamina glia in shaping the postsynaptic response.

Previous evidence had already clearly implicated HCLA as a subunit of the native channel (Gengs et al., 2002). It is required for synaptic transmission at the photoreceptor–LMC synapse and for orientation and motion vision (Rister et al., 2007). However, contradictory reports on the channels' properties and localization left the role of HCLB unclear. In particular, previous measurements of the D–R profiles of the two channels led to widely discrepant EC_{50} values (Table 1), none of which could be identified with the native receptor (Skingsley et al., 1995). The most conspicuous discrepancy concerned the EC_{50} value for HCLA, with the value of 166 μM reported by Gisselmann et al. (2002) an order of magnitude larger than that found by Zheng et al. (2002), despite using the same expression system (*Xenopus* oocytes). In this respect, it is interesting to note that the cDNA used by Gisselmann et al. (2002) lacked a region of 5′UTR present in both the cDNA construct used in this study and that of Zheng et al. (2002). This region includes 8 nt (−276 to −269) that are deleted in ort^{P306} and that underlie its (non-null) mutant phenotype (Gengs et al., 2002). Intriguingly, our earlier recordings of the native receptor in LMCs from ort^{P306} yielded an EC_{50} of 190 μM (Gengs et al., 2002), representing a close match with Gisselmann et al. (2002)'s estimate. Although this may be coincidental, it may indicate the

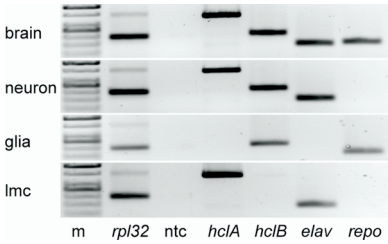

Figure 7. Expression profile of *hclA* and *hclB* determined by mRNA tagging. Shown is a RT-PCR gel using primers for *hclA* and *hclB*, as well as *elav* and *repo* controls (to identify neurons and glia, respectively) and *rpl32* ("housekeeping" control). All transcripts were detected in whole-brain tissue using conventional RT-PCR (top row). mRNA immunoprecipitated from all neurons using *elav-Gal4* × *UAS-hPF* included both *hclA* and *hclB* transcripts, as well as *elav* (positive control); the lack of *repo* signal (negative control) confirms that there was no contaminating signal. Glial mRNA (using *repo-gal4*) contained *hclB* (and *repo*) but no *hclA* (or *elav*). In the LMCs (*L2-Gal4*), only *hclA* and *elav* were detected. All samples expressed the general housekeeping control gene *rpl32* (ribosomal protein). ntc, No template control; m, markers.

generation of an unrecognized splice variant under control of this region of the 5′UTR.

In the present study, we examined the properties of HCLA and HCLB expressed in *Drosophila* S2 cells, and found that HCLA homomers ($EC_{50} = 25\ \mu M$; $n_H = 2.6$) were an excellent match for the native receptor (24 μM; $n_H = 2.5$). Although we cannot exclude the possibility that channel properties are modified by the different cellular environments, our recordings were made under very similar conditions to previous recordings of the native receptors from dissociated LMCs, and we interpret this equivalence as strong evidence for the identity of the native receptor as HCLA homomers. Our results from HCLB homomers and HCLA/B cotransfectants were broadly similar to previous results (Tables 1, 2). Notably, all studies agree that HCLA/HCLB heteromers have distinctly higher HA sensitivity than either HCLA or HCLB homomers, as well as native LMC receptors, providing compelling evidence that these subunits can assemble into functional heteromers, but suggesting that they do not contribute to the native channels on the LMCs.

Analysis of single-channel properties provided additional strong evidence for the identity of the native receptor as an HCLA homomer. The single-channel conductance of both HCLB homomers and heteromeric receptors (~4 pS estimated by noise analysis) was an order of magnitude smaller than that of the native channels (Skingsley et al., 1995). This suggests a dominant conductance-limiting effect brought about by HCLB subunits to the receptor it is part of, be it an HCLB homomer or an HCLA/HCLB heteromer. In contrast, HCLA homomers had very similar properties to those of the native receptor. This extended to a close agreement of three distinct conductance states (~25, 40, and 60 pS), with similar weighting and open times (Table 4). An unusual feature common to both receptors was the disappearance of the largest conductance level at positive holding potentials. LMCs are not thought to depolarize above +20 mV (Hardie and Weckström, 1990), so the physiological significance of this feature, if any, is unclear. However, because this phenomenon has not been reported for other Cys-loop LGICs, it stands as further strong evidence for the identity of native receptors as HCLA homomers and an intriguing feature for future investigation.

The functional equivalence of their electrophysiological properties suggests that HCLA homomers are sufficient to account for the properties of the native receptor. The absence of ERG transients in the null *hclA* (*ort*) mutant also clearly showed that HCLA is required for synaptic transmission to the LMCs. In contrast, robust transients remained in null *hclB* (*hisCl1*^{134}) mutants. Surprisingly however, the "on" transients in ERGs from *hisCl1*^{134} mutants were actually enhanced compared with wild type, whereas recordings from LMCs revealed significantly slower responses that saturated over a smaller dynamic range. In principle, these phenotypes might be interpreted as evidence for a contribution of HCLB to the native channels. However, because our electrophysiological analysis did not support this, we investigated the cellular localization of the respective channels. Previous reports of HCLB localization are equivocal. Zheng et al. (2002) reported that *hclA* and *hclB* transcripts were both predominantly expressed in eye tissue at comparable levels However, other studies using *in situ* hybridization failed to detect *hclB* RNA in any brain tissue, while confirming expression of *hclA* in the lamina (Gisselmann et al., 2002; Witte et al., 2002). More recently, HCLA, but not HCLB, was localized in the lamina by immunocytochemistry (Hong et al., 2006). In the present study, we achieved higher resolution using a reporter gene strategy. We confirmed expression of *hclA* in the LMCs, and probably amacrine cells, but found that, within the lamina, the *hclB* enhancer drove expression exclusively in glial cells (Fig. 6). This conclusion was fully substantiated by an independent approach using mRNA tagging (Fig. 7).

It has long been known that the lamina glia receive direct synaptic input from photoreceptors via the same tetradic synapses that innervate the LMCs (Burkhardt and Braitenberg, 1976; Shaw, 1984; Meinertzhagen and O'Neil, 1991), but the role of this glial synapse was unknown. Our finding of altered LMC responses in *hclB* mutants now implies that the glia play a subtle but significant role in shaping the LMC response. Intracellular recordings have never been made from these glia, so we can only speculate as to how this might be achieved. One possibility would be by contributing to extracellular field potentials, which are believed to be important for determining the effective transmembrane potential (and hence transmitter release) at the photoreceptor synapse (Shaw, 1984). Another would be competition for transmitter binding between LMC and glia postsynaptic histamine receptors, which share the same synaptic cleft at the tetradic synapses.

Surprisingly, the "on" transients in the *hclB* mutant ERG were substantially enhanced compared with control flies. A possible explanation for this unexpected phenotype derives from the fact that the ERG represents a low-pass filtered signal of the underlying neural responses. Because LMC responses in the *hclB* mutants had approximately twofold slower kinetics (Fig. 5), they should suffer less attenuation in the resultant ERG. To estimate the extent of the low-pass filtering, we compared the kinetics of intracellular LMC responses and ERGs recorded with identical stimulation. At low intensities, at which the ERG is dominated by the LMC contribution, the wild-type ERG "on" transient peaks ~50–60 ms after light onset, whereas the LMC response peaks much earlier (25–30 ms). By digitally filtering LMC responses, we found that such a delay would be generated by an RC filter of ~20 Hz. When LMC responses from wild-type and *hclB* (*hisCl1*^{134}) mutants were filtered in a similar manner, wild-type peak amplitudes were attenuated approximately twofold to threefold, whereas the slower mutant responses suffered only minor (~30%) attenuation. Potentially, this could fully account for the approximately twofold enhanced ERG transients in *hclB* mutants; however, we cannot exclude other contributory factors. For example, one would expect that the HCLB-mediated signal in the glia also contributes to the ERG; loss of this signal could in principle enhance the "on" transients if the glia response was depo-

larizing (although this would require the chloride reversal potential in the glia to be positive to resting potential). In addition, the amplitude of extracellularly recorded responses is critically dependent on resistance barriers in the surrounding tissue. Because the glial cells form a sheath surrounding each cartridge in the lamina, they are likely to make a significant contribution to such resistance barriers, which might be expected to be increased in the absence of their only known synaptic conductance (HCLB).

In conclusion, the loss of synaptic transients in ERGs of null *hclA* mutants indicates that HCLA is an essential component of the synaptic receptor, whereas the striking quantitative similarity between the properties of HCLA homomers and the native receptor strongly suggests their functional equivalence. Along with evidence showing lack of HCLB expression in the LMCs, we consequently propose that the native LMC receptor is composed of HCLA homomeric channels. We further suggest that the *hclB* (*hiscl1*) phenotypes observed in the ERG and intracellular LMC recordings reflect a previously unrecognized contribution of the lamina glia to signaling at the photoreceptor synapse.

References

Buchner E (1991) Genes expressed in the adult brain of *Drosophila* and effects of their mutations on behavior: a survey of transmitter- and second messenger-related genes. J Neurogenet 7:153–192.

Buchner E, Buchner S, Burg MG, Hofbauer A, Pak WL, Pollack I (1993) Histamine is a major mechanosensory neurotransmitter candidate in *Drosophila melanogaster*. Cell Tissue Res 273:119–125.

Burkhardt W, Braitenberg V (1976) Some peculiar synaptic complexes in the first visual ganglion of the fly, *Musca domestica*. Cell Tissue Res 173:287–308.

Callaway JC, Stuart AE (1989) Biochemical and physiological evidence that histamine is the transmitter of barnacle photoreceptors. Vis Neurosci 3:311–325.

Colquhoun D, Hawkes AG (1977) Relaxation and fluctuations of membrane currents that flow through drug-operated channels. Proc R Soc Lond B Biol Sci 199:231–262.

Coombe PE (1986) The large monopolar cells L1 and L2 are responsible for ERG transients in *Drosophila*. J Comp Physiol A Neuroethol Sens Neural Behav Physiol 159:655–665.

Elias MS, Evans PD (1983) Histamine in the insect nervous system: distribution, synthesis and metabolism. J Neurochem 41:562–568.

Franz O, Bruchhaus I, Roeder T (1999) Verification of differential gene transcription using virtual northern blotting. Nucleic Acids Res 27:e3.

Gengs C, Leung HT, Skingsley DR, Iovchev MI, Yin Z, Semenov EP, Burg MG, Hardie RC, Pak WL (2002) The target of *Drosophila* photoreceptor synaptic transmission is a histamine-gated chloride channel encoded by *ort* (*hclA*). J Biol Chem 277:42113–42120.

Gisselmann G, Pusch H, Hovemann BT, Hatt H (2002) Two cDNAs coding for histamine-gated ion channels in *D. melanogaster*. Nat Neurosci 5:11–12.

Gisselmann G, Plonka J, Pusch H, Hatt H (2004) Unusual functional properties of homo- and heteromultimeric histamine-gated chloride channels of *Drosophila melanogaster*: spontaneous currents and dual gating by GABA and histamine. Neurosci Lett 372:151–156.

Hardie RC (1987) Is histamine a neurotransmitter in insect photoreceptors? J Comp Physiol A Neuroethol Sens Neural Behav Physiol 161:201–213.

Hardie RC (1989a) Neurotransmitters in compound eyes. In: Facets of vision (Stavenga DG, Hardie RC, eds), pp 235–256. Berlin: Springer.

Hardie RC (1989b) A histamine-activated chloride channel involved in neurotransmission at a photoreceptor synapse. Nature 339:704–706.

Hardie RC, Weckström M (1990) Three classes of potassium channels in identified non-spiking visual interneurones from the blowfly *Calliphora vicina*. J Comp Physiol A Neuroethol Sens Neural Behav Physiol 167:723–736.

Hardie RC, Reuss H, Lansdell SJ, Millar NS (1997) Functional equivalence of native light-sensitive channels in the *Drosophila trp*^{301} mutant and TRPL cation channels expressed in a stably transfected *Drosophila* cell line. Cell Calcium 21:431–440.

Heisenberg M (1971) Separation of receptor and lamina potentials in the electroretinogram of normal and mutant *Drosophila*. J Exp Biol 55:85–100.

Hong S-T, Bang S, Paik D, Kang J, Hwang S, Jeon K, Chun B, Hyun S, Lee Y, Kim J (2006) Histamine and its receptors modulate temperature-preference behaviors in *Drosophila*. J Neurosci 26:7245–7256.

Järvilehto M, Zettler F (1971) Localized intracellular potentials from pre- and postsynaptic components in the external plexiform layer of an insect retina. Z Vergl Physiol 75:422–440.

Juusola M, Hardie RC (2001) Light adaptation in *Drosophila* photoreceptors: I. Response dynamics and signaling efficiency at 25 degrees C. J Gen Physiol 117:3–25.

Laughlin SB, Howard J, Blakeslee B (1987) Synaptic limitations to contrast coding in the retina of the blowfly *Calliphora*. Proc R Soc Lond B Biol Sci 231:437–467.

Meinertzhagen IA, O'Neil SD (1991) Synaptic organization of columnar elements in the lamina of the wild type in *Drosophila* melanogaster. J Comp Neurol 305:232–263.

Millar NS, Baylis HA, Reaper C, Bunting R, Mason WT, Sattelle DB (1995) Functional expression of a cloned *Drosophila* muscarinic acetylcholine receptor in a stable *Drosophila* cell line. J Exp Biol 198:1843–1850.

Nicol D, Meinertzhagen IA (1982) An analysis of the number and composition of the synaptic populations formed by photoreceptors of the fly. J Comp Neurol 207:29–44.

O'Tousa JE, Leonard DS, Pak WL (1989) Morphological defects in *ora*^{JK84} photoreceptors caused by mutation in R1–6 opsin gene of *Drosophila*. J Neurogenet 6:41–52.

Rajaram S, Scott RL, Nash HA (2005) Retrograde signaling from the brain to the retina modulates the termination of the light response in *Drosophila*. Proc Natl Acad Sci U S A 102:17840–17845.

Rister J, Pauls D, Schnell B, Ting CY, Lee CH, Sinakevitch I, Morante J, Strausfeld NJ, Ito K, Heisenberg M (2007) Dissection of the peripheral motion channel in the visual system of *Drosophila melanogaster*. Neuron 56:155–170.

Sarthy PV (1991) Histamine: a neurotransmitter candidate for *Drosophila* photoreceptors. J Neurochem 57:1757–1768.

Schneider I (1972) Cell lines derived from late embryonic stages of *Drosophila melanogaster*. J Embryol Exp Morphol 27:353–365.

Sharma Y, Cheung U, Larsen EW, Eberl DF (2002) PPTGAL, a convenient Gal4 P-element vector for testing expression of enhancer fragments in *Drosophila*. Genesis 34:115–118.

Shaw SR (1984) Early visual processing in insects. J Exp Biol 112:225–251.

Skingsley DR, Laughlin SB, Hardie RC (1995) Properties of histamine-activated chloride channels in the large monopolar cells of the dipteran compound eye—a comparative-study. J Comp Physiol A Neuroethol Sens Neural Behav Physiol 176:611–623.

Spradling AC, Rubin GM (1982) Transposition of cloned P elements into *Drosophila* germ line chromosomes. Science 218:341–347.

Strausfeld NJ, Nässel DR (1980) Neuroarchitecture of brain regions that subserve the compound eyes of crustacea and insects. In: Handbook of sensory physiology, Vol II/6B (Autrum H, ed), pp 1–133. Heidelberg: Springer.

Stuart AE (1999) From fruit flies to barnacles, histamine is the neurotransmitter of arthropod photoreceptors. Neuron 22:431–433.

Stuart AE, Borycz J, Meinertzhagen IA (2007) The dynamics of signaling at the histaminergic photoreceptor synapse of arthropods. Prog Neurobiol 82:202–227.

Witte I, Kreienkamp HJ, Gewecke M, Roeder T (2002) Putative histamine-gated chloride channel subunits of the insect visual system and thoracic ganglion. J Neurochem 83:504–514.

Yang Z, Edenberg HJ, Davis RL (2005) Isolation of mRNA from specific tissues of *Drosophila* by mRNA tagging. Nucleic Acids Res 33:e148.

Zheng L, de Polavieja GG, Wolfram V, Asyali MH, Hardie RC, Juusola M (2006) Feedback network controls photoreceptor output at the layer of first visual synapses in *Drosophila*. J Gen Physiol 127:495–510.

Zheng Y, Hirschberg B, Yuan J, Wang AP, Hunt DC, Ludmerer SW, Schmatz DM, Cully DF (2002) Identification of two novel *Drosophila melanogaster* histamine-gated chloride channel subunits expressed in the eye. J Biol Chem 277:2000–2005.